AIAA AVIATION Forum
August 2-6, 2021, VIRTUAL EVENT
AIAA AVIATION 2021 FORUM

10.2514/6.2021-2290

Non-linear Forchheimer corrections in acoustic scattering

Matthew J. Colbrook * and Lorna J. Ayton†
Department of Applied Mathematics and Theoretical Physics, University of Cambridge

We present a fast numerical method for predicting the aerodynamic noise generated by foam-like porous aerofoils. Darcy's law, describing the pressure jump across the aerofoil, may be unsuitable in such situations, particularly for high-frequency noise sources where the unsteady velocity fluctuations are large relative to the porous structure size. We therefore introduce an inertial Forchheimer correction that results in a non-linear boundary condition relating the pressure jump across the material to the fluid displacement. Based on local Mathieu function expansions, we provide a semi-analytical boundary spectral method that is well-suited to both linear and non-linear boundary conditions. In the latter case, Newton's method is employed to solve the resulting non-linear system of equations. The outcome is a fast semi-analytical model that incorporates such non-linear effects without requiring a full turbulent simulation. Whilst we consider only the simplified case of scattering by a thin porous aerofoil with no background flow, when the non-linear inertial correction is included good agreement is seen between the model predictions and experimental results. A key conclusion is that for sufficiently low-permeability materials, the effects of inertia can outweigh the noise attenuation effects of viscosity. This helps explain the discrepancy between experimental results and previous (linear) low-fidelity numerical simulations or analytical predictions, which typically overestimate the noise reduction capabilities of porous aerofoils.

I. Introduction

Controlling aerofoil-interaction noise through porosity has become increasingly popular over recent years [1–5]. Currently there are two main notions within this body of research. The first arises for thin perforated plates [4, 5], where apertures fully puncture the material. In the case of no background steady flow, the apertures induce an acoustic (Rayleigh) conductivity on the surface [6]. When there is a background flow (tangential [7] or bias [8]), the generated vorticity acts dissipatively. Both mechanisms are captured by the Rayleigh conductivity parameter, K_R, whose real part corresponds to conductivity and whose imaginary part to dissipation. The acoustic pressure, $pe^{-\mathrm{i}\omega t}$ (where the factor $e^{-\mathrm{i}\omega t}$ will be suppressed throughout), on a thin plate lying in $y = 0$ must satisfy the condition

$$K_R[p] = \mathrm{i}\rho_f \omega v,$$

where ρ_f is the external fluid density and v is the normal fluid velocity averaged over a unit area of the surface. We use the notation $p(x, 0+)$ and $p(x, 0-)$ to denote the values of the pressure field just above and just below the plate respectively, and define $[p](x) = p(x, 0+) - p(x, 0-)$. This condition is valid only when the open area of the plate is sufficiently small (low porosity) and the wavenumber is much smaller than the reciprocal of a typical pore radius [7].

The second notion of porosity arises for materials such as metal foams [1, 9], where microscopic void spaces are found within a rigid framework. Here, the local Reynolds number is low and viscous dissipation plays a dominant role. For sufficiently low local Reynolds numbers ($Re_L < 1$), only the viscous dissipation is important, and the pressure jump across these materials may be described linearly by Darcy's Law,

$$K\frac{[p]}{h} = -\mu v,$$

where μ is the air viscosity, K is the permeability of the material and h is the small height over which the pressure jump is taken. However, at higher local Reynolds numbers ($1 < Re_L < 10$), a correction for inertial effects should be included, and the pressure difference may be described by the non-linear boundary Forchheimer equation [10],

$$K\frac{[p]}{h} = -\mu v - \beta\rho_f \sqrt{K}\, v|v|,$$

*Junior Research Fellow, Department of Applied Mathematics and Theoretical Physics, University of Cambridge, email: m.colbrook@damtp.cam.ac.uk
†EPSRC Early Career Fellow, Department of Applied Mathematics and Theoretical Physics, University of Cambridge, email: l.j.ayton@damtp.cam.ac.uk

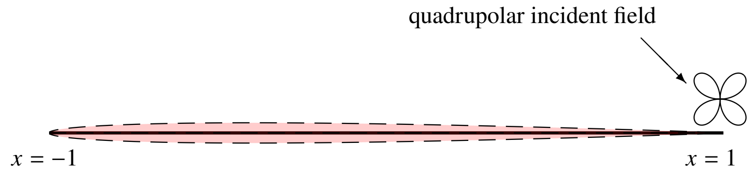

Fig. 1 Schematic of the single plate $\{(x, 0) : -1 \leq x \leq 1\}$ (zero-thickness approximation) with a quadrupolar source. The shaded area corresponds to $h(x)$ of an NACA 4-digit aerofoil with 6% thickness.

where β is the inertial coefficient. The nature of this boundary condition still permits the time-harmonic form $\sim e^{-\mathrm{i}\omega t}$.

Previous theoretical [5] and low-fidelity numerical [11] work focuses on the first notion of porosity (perforated plates). These models do not include a background flow and consider the boundary conditions to be linearised to $y = 0$, thus effectively reducing an aerofoil to a flat plate. For both perforations and foam-like materials [3, 4], experimental findings show that porosity is effective at reducing low and mid-frequency noise. Moreover, theoretical and low-fidelity linear numerical models can capture this feature. However, these models often *overpredict* the potential reduction of noise. Few models consider foam-like porous aerofoils, despite these being commonplace in the experimental literature. At high frequencies for these foam-like materials, the local Reynolds number can be sufficiently high within the material to require the inclusion of the non-linear Forchheimer correction.

The goal of this paper is to investigate the effect of this non-linear inertial term on the acoustic scattering by thin porous aerofoils. We provide a fast, semi-analytical model that incorporates the non-linear effects of the Forchheimer model without requiring a full turbulent simulation. To do this, we extend a previous linear boundary collocation method [11–14] based on local Mathieu function expansions. A partitioning of the system according to the different (kinematic and non-linear Forchheimer) boundary conditions, gives rise to a non-linear system of equations (see (10)) for the unknown coefficients, which we solve via Newton's method. The result is a boundary spectral method that can deal with the non-linear Forchheimer correction, and more general non-linear boundary conditions, efficiently and accurately for a wide range of parameters. Whilst the physical model is simplified to consider just the scattering by a thin porous aerofoil with no background flow, good agreement is seen between the model predictions and experimental results when the non-linear inertial correction is included. It is found that for sufficiently low-permeability materials, the effects of inertia can outweigh the noise attenuation effects of viscosity. This helps explain the discrepancy between experimental results and previous (linear) low-fidelity numerical simulations or analytical predictions, which typically overestimate the noise reduction capabilities of porous aerofoils. Code for the numerical method can be found at [15].

II. Mathematical Model

Suppose that an acoustic source of pressure p_{I} interacts with a plate $\{(x, 0) : -1 \leq x \leq 1\}$ (lengths have been non-dimensionalised by the semi-chord, d). The thickness of the plate, $h(x)$, which is permitted to vary in the x direction, is constrained to be much smaller than the semichord, $h(x) \ll 1$, and hence we consider the zero-thickness approximation (see Figure 1). The scattered field has pressure denoted by p. We assume that p and p_{I} have the usual time dependence $\mathrm{e}^{-\mathrm{i}\omega t}$ (omitted throughout) and therefore p satisfies the Helmholtz equation

$$\left(\frac{\partial}{\partial x^2} + \frac{\partial}{\partial y^2} + k_0^2\right) p = 0, \quad k_0 = \omega / c_0$$

where pressure has been non-dimensionalised by $\rho_f c_0^2$ and c_0 is the speed of sound. For example, we shall focus on a near-field quadrupole sound source corresponding to

$$p_{\mathrm{I}}(x, y) = P_0 \frac{\mathrm{i}k_0^2}{4r_0^2}(x - x_0)(y - y_0) H_2^{(1)}(k_0 r_0), \tag{1}$$

where (x_0, y_0) is the source location, $r_0(x, y) = \sqrt{(x - x_0)^2 + (y - y_0)^2}$, and $H_n^{(1)}$ denotes the nth order Hankel function of the first kind. We mention, however, that an arbitrary acoustic source could just as easily be used. In an aerodynamic setting, the principle source of noise arises from quadrupole type sources, $\sim \frac{\partial T_{ij}}{\partial x_i x_j}$, as described by Lighthill [16], where

$T_{ij} = \rho u_i u_j$ is the Lighthill tensor, with ρ and $u_{i,j}$ the typical (dimensional) density and (dimensional) velocities of the turbulent flow. We therefore allocate a (non-dimensionalised) scaling of the quadrupole corresponding to $P_0 = M^2$, where M is the (low) Mach number of the flow local to the quadrupole.

The (non-dimensionalised) average fluid displacement normal to the plate is denoted by η_a. Therefore, the non-dimensionalised kinematic condition on the plate takes the form

$$\frac{\partial p}{\partial y}\Big|_{y=0} + \frac{\partial p_{\mathrm{I}}}{\partial y}\Big|_{y=0} = C_0(x)\eta_a|_{y=0}, \qquad |x| < 1, \tag{2}$$

with $C_0(x) = k_0^2$. Here we have neglected $O(h)$ terms arising from the small thickness of the plate allowing us to present a condition along $y = 0$. The non-linear Forchheimer condition (taking only leading order in h) is

$$[p] = C_1(x)\eta_a + C_2(x)\eta_a|\eta_a|, \qquad |x| < 1, \tag{3}$$

where $C_1(x) = \mathrm{i}k_0 h(x)/G_{rn}$, and $C_2(x) = \mathrm{i}G_{rf}\, h(x) k_0^2/G_{rn}$ are defined in terms of $G_{rn} = \rho_f K c_0/(\mu d)$, and $G_{rf} = \rho_f \beta c_0 \sqrt{K}/\mu$ [10]. The solution p is also required to satisfy the Sommerfeld radiation condition for outgoing waves at infinity. Finally, we have written the boundary conditions (2) and (3) in a general form with coefficients $C_{0,1,2}$, since the collocation method can deal with this generality. However, our focus will be on the above specified values of C_i throughout. Additionally, the method can be extended to different non-linear couplings in (3), for example, sums of terms involving $\eta_a|\eta_a|^\alpha$ for $\alpha \geq -1$ or higher-order corrections.

III. Method of Solution

A. The general solution

We introduce elliptic coordinates via $x = \cosh(\nu)\cos(\tau)$, $y = \sinh(\nu)\sin(\tau)$, where, with an abuse of notation, we write functions of (x, y) also as functions of (ν, τ). To simplify the formulae, we let $Q = k_0^2/4$. Separation of variables leads to the expansion

$$p(\nu, \tau) = \sum_{m=1}^{\infty} a_m \mathrm{se}_m(\tau)\mathrm{Hse}_m(\nu), \tag{4}$$

where $\mathrm{se}_m(\tau) = \mathrm{se}_m(Q; \tau)$ denote sine-elliptic functions and $\mathrm{Hse}_m(Q; \nu) = \mathrm{Hse}_m(\nu)$ denote Mathieu–Hankel functions. Full details of this process can be found in, for example, [12, 13, 17]. For example, numerical evaluations can be achieved by expanding se_m is sine functions and Hse_m in Bessel functions. We choose the normalisation such that $\mathrm{Hse}_m'(0) = 1$.

We use the boundary conditions to solve for the unknown coefficients a_m, after which the solution can be evaluated anywhere in the (x, y) plane. Of particular interest is the far-field directivity, $D(\theta)$, which is defined via

$$p(r, \theta) \sim D(\theta)\frac{\mathrm{e}^{\mathrm{i}wr}}{\sqrt{r}}, \qquad \text{as} \qquad r \to \infty,$$

where (r, θ) are the usual polar coordinates. Given the Bessel function expansions of $\mathrm{Hse}_m(\nu)$, we can directly compute $D(\theta)$ from (4) using asymptotics of Bessel functions to obtain

$$D(\theta) = \sqrt{\frac{2}{\pi k_0}} \sum_{m=1}^{\infty} a_m \lambda_m(Q)\mathrm{se}_m(\theta),$$

for easily computed constants $\lambda_m(Q)$. This allows easy computation of the scattered far-field sound (in dB):

$$P = 10\log_{10}\left(\int_0^{2\pi} |D(\theta)|^2 d\theta\right). \tag{5}$$

B. Collocating the boundary conditions

We adopt a spectral collocation approach to finding the unknown coefficients in the expansion (4). Throughout, we denote the approximate coefficients by $\tilde{a}_m$. We truncate the expansion (4) to M terms and supplement the expansion of

p with an expansion of η_a in terms of Chebyshev polynomials of the first kind

$$\eta_a(x) = \sum_{j=0}^{\infty} b_j T_j(x).$$

We truncate this expansion to N terms for approximate coefficients $\tilde{b}_j$. The kinematic relation (2) becomes

$$\sqrt{1-x^2} \cdot \frac{\partial p_{\mathrm{I}}}{\partial y}(x) + \sum_{m=1}^{M} \tilde{a}_m \mathrm{se}_m\left(\cos^{-1}(x)\right) = \sqrt{1-x^2} \cdot C_0(x) \sum_{j=0}^{N-1} \tilde{b}_j T_j(x). \tag{6}$$

We collocate (6) at the Chebyshev points $\{\cos((2j-1)\pi/(2M)) : j = 1, ..., M\}$. The non-linear coupling (3) yields

$$2\sum_{m=1}^{M} \tilde{a}_m \mathrm{se}_m\left(\cos^{-1}(x)\right) \mathrm{Hse}_m(0) = \left[C_1(x) + C_2(x)\left|\sum_{j=0}^{N-1} \tilde{b}_j T_j(x)\right|\right]\left[\sum_{j=0}^{N-1} \tilde{b}_j T_j(x)\right], \tag{7}$$

which we collocate at N Chebyshev points. Coupling (6) and (7) leads to the non-linear equation

$$Av + (Bv) \circ |Cv| = c, \tag{8}$$

where $A, B, C \in \mathbb{C}^{(M+N)\times(M+N)}$, v is the concatenated vector of the unknown coefficients $\{\tilde{a}_m, \tilde{b}_j : m = 1, ..., M, j = 0, ..., N-1\}$, c denotes the forcing that arises from the $\partial_y p_{\mathrm{I}}$ term in (6), $\circ$ denotes component-wise multiplication of vectors, and the absolute value is taken component-wise.

C. Solving the non-linear system

To solve the discretised equation (8), we apply Newton's method. We partition the unknown coefficients into first the M unknown coefficients $\{\tilde{a}_m\}$ and then the N unknown coefficients $\{\tilde{b}_j\}$, and the collocation points into the kinematic conditions and then the non-linear couplings. This yields the following block structure of the matrices A, B and C, and the vectors v and c:

$$A = \left(\begin{array}{c|c} A_{11} & A_{12} \\ \hline A_{21} & A_{22} \end{array}\right), B = \left(\begin{array}{c|c} 0 & 0 \\ \hline 0 & B_{22} \end{array}\right), C = \left(\begin{array}{c|c} 0 & 0 \\ \hline 0 & C_{22} \end{array}\right), v = \left(\begin{array}{c} v_1 \\ \hline v_2 \end{array}\right), c = \left(\begin{array}{c} c_1 \\ \hline 0 \end{array}\right).$$

By considering the rows corresponding to collocating the kinematic condition, this yields the relation

$$v_1 = A_{11}^{-1}(c_1 - A_{12}v_2). \tag{9}$$

Substituting this into the non-linear coupling yields

$$\left[A_{22} - A_{21}A_{11}^{-1}A_{12}\right] v_2 + (B_{22}v_2) \circ |C_{22}v_2| = -A_{21}A_{11}^{-1}c_1. \tag{10}$$

We solve (10) via Newton's method. To do this we split vectors into real and imaginary parts so that taking absolute values is differentiable almost everywhere. We also choose the linearised solution (obtained by setting $B_{22} = 0$) as our initial vector. We cannot rule out the possibility of multiple solutions to the non-linear system of equations (10). In the case of multiple solutions, we expect the physically correct solution to be the one closest to the linearised solution. However, in the following examples we checked for additional solutions using deflation and were unable to find any. This provides numerical evidence (though not a mathematical proof) that there is a unique solution to (10). Once v_2 is computed, v_1 is computed via (9). Note that using the decompositions reduces the dimensions of the linear systems we solve at each iteration of Newton's method from $(2M+2N)\times(2M+2N)$ to $(2N)\times(2N)$ (the factors of two arise from splitting into real and imaginary parts). Since the linear systems are dense, for the choice of $M = N$, and ignoring the difference in the number of iterations of Newton's method, this leads to a roughly eightfold speed-up for large $M = N$.

D. Numerical Convergence

In this section, we show convergence of our numerical method, taking $M = N$ throughout. We compute the relative error of P (given by (5)), as well as the relative error of $[p]$ along the plate (measured in the L^2 norm using a large

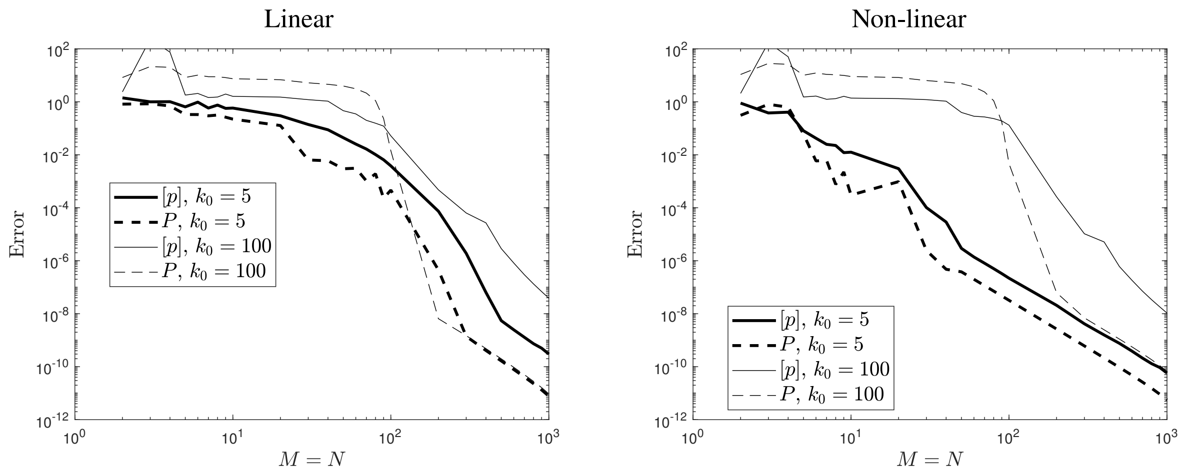

Fig. 2 Convergence of the method for the linear case (left) and non-linear case (right).

Case	K (m^2)	β	Material	Ref.
1	0	-	Impermeable	-
2	2.7×10^{-9}	0.14	Alantum NiCrAl open-cell metal foam	[9]
3	5.72×10^{-11}	$0.5^{\dagger}$	Sintered PE granulate (Porex)	[1, 3]
4	3.65×10^{-12}	0.613	Sintered SUS316L powder (Group 2, 9mm)	[18]

Table 1 Summary of test cases. †No inertial parameter specified; we have selected an inertial parameter close to that of the sintered material of Case 4.

number of discrete points), by comparing to a larger value of $M = N$. We tested the numerical method extensively, and for all cases, we found similar behaviour to the following examples.

To demonstrate generality, we consider the case of

$$C_0(x) = k_0^2, \quad C_1(x) = \mathrm{i}k_0(1.2 + \sin(20x)), \quad C_2(x) = \mathrm{i}20k_0^2(x^2 + 1),$$

where C_2 is set to zero for the linear case. The pressure due to the acoustic source is taken to be a plane wave of unit amplitude incident at angle $\pi/3$. Figure 2 shows the convergence for $k_0 = 5$ and $k_0 = 100$. We see that in both cases we can obtain a relative accuracy of at least 10^{-7} for $[p]$ and 10^{-10} for P, for $M = N = 1000$. We also see that, for a given accuracy, a smaller number of basis functions are needed for a smaller k_0. Consistent with the linear case in previous works, there is a value of $M = N$ (typically of the order k_0) after which the convergence rate increases (particularly visible in the P error curves), before settling to an algebraic rate for large $M = N$.

IV. Results

Parameters are set as standard for air: $\rho = 1.225\text{kgm}^{-3}$, $c_0 = 343\text{ms}^{-1}$, $\mu = 1.81 \times 10^{-5}\text{Pa s}$, and we shall use a semichord length of 75mm, which is in line with small-scale experimental wind tunnel tests [1, 4, 9]. We obtain a number of test case parameters for K and β from [1, 9, 18], which are summarised in Table 1.

First, we compare the linear and non-linear prediction for noise generated by a quadrupole close to the trailing edge of a plate of uniform thickness of 0.9mm corresponding to a non-dimensionalised thickness of $h(x) = 0.012$. This thickness is much larger than the characteristic size of the selected materials in Table 1, which vary from $\sim 50 - 800\mu$m. The quadrupole is placed at $(0.99, 0.1)$, corresponding to a vertical height of 5% chordlength. When considering Case 2, we alter C_0 to

$$C_0(x) = \begin{cases} 0, & \text{if } x \leq 0.6, \\ k_0^2, & \text{otherwise,} \end{cases}$$

in order to more accurately model the setup of [9]. There, an impermeable aerofoil had porous inserts appended to the trailing edge, resulting in potential junction noise (at the impermeable-permeable junction).

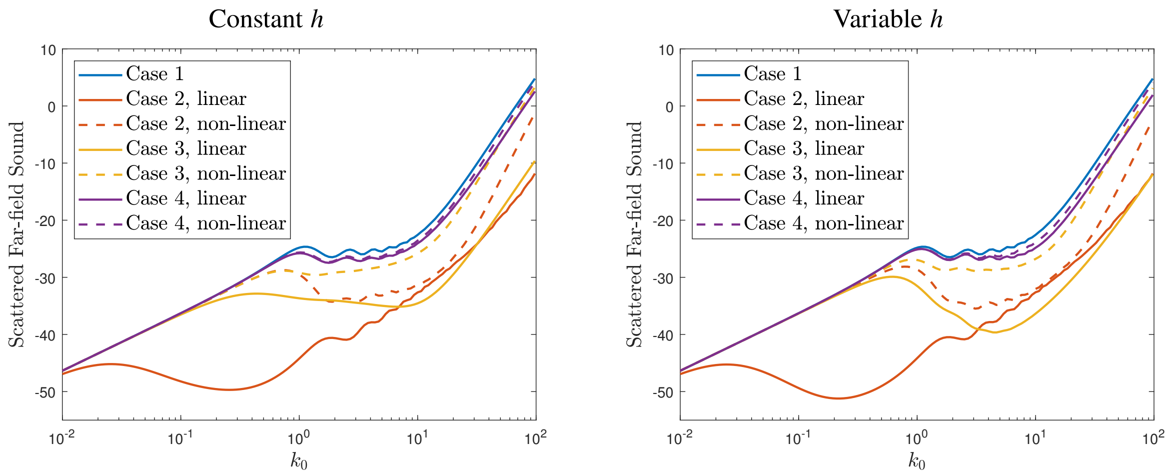

Fig. 3 Far-field sound across a range of frequencies for each Case. Left: Results for non-dimensionalised thickness of $h(x) = 0.012$. Right: Results for an NACA 4-digit aerofoil with 6% thickness.

Figure 3 (left) illustrates the non-dimensional scattered far-field sound, defined in (5), for our four cases. Case 1 is the reference impermeable case. We see that for low permeability (Case 4) there is little difference between the linear and non-linear predictions over the whole frequency range, and such a low permeability does not produce a significant noise reduction versus the impermeable Case 1. As permeability increases, the noise reduction versus the impermeable plate increases but so too does the difference between the linear and non-linear results for mid and high frequencies. Thus, for higher permeability, inertial effects can become significant on the generation of aerodynamic noise. The particular metal foam for Case 2 has the largest pores $\sim 800\mu$m, thus the largest local Reynolds number. It is therefore expected that the non-linear effects should be greatest in this case [10].

The maximum noise reduction observed by Rubio Carpio et al. [9] for Case 2 was 10dB, and a noise increase of $\sim$ 8dB was observed at high frequencies. The linear prediction hugely overestimates the noise reduction and does not capture any possible noise increase, whereas the non-linear model predicts a similar $\sim$ 10dB noise reduction. As frequency increases, the noise reduction does diminish for the non-linear case, although an increase is not seen. The high-frequency noise increase in the results of [9] is dominated by roughness noise. Hence, we do not expect to capture this feature in our model. Furthermore, for this case, the local Reynolds number is $Re_L \sim 54\omega\eta_a$, where $\omega\eta_a$ is the local flow speed. This highly porous material constructed from large cells may therefore exceed the limit of validity of the Forchheimer model ($1 < Re_L < 10$, [10]). Nevertheless, the results indicate a reasonable comparison to [9].

Cases 3 has a lower local Reynolds number than Case 2 due to smaller pore sizes and thus should be better described by the Forchheimer model. The acoustic results from Geyer et al. [1] for Case 3 indicate a maximum noise reduction of $\sim$ 6dB, and a noise increase at higher frequencies. Our non-linear model again captures a similar maximum noise reduction, and trends towards a noise increase at high frequencies. Of course, this model still excludes any surface roughness noise, which becomes important at high frequencies. However, we can see that not all of the noise increase at high frequencies can be directly attributed to surface roughness, and some should be attributed to inertial (non-linear) effects. The noise increase observed in Geyer et al.'s data [1] at low frequencies is a narrow spectral peak that is attributed to trailing-edge bluntness noise which is not captured in our model. Thus we do not observe a similar peak in our results.

Case 4 has the lowest local Reynolds number and lowest permeability. Thus the effects of inertia should be weakest. Indeed this is observed in our results since the linear and non-linear predictions differ only by $\sim$ 1dB. The defined porosity of the material in Case 4 is close to 50% (Cases 2 and 3 have higher porosities). Therefore, we anticipate that for materials with porosities lower than $\sim$ 50%, the linear Darcy model would be suitable. However, for materials with greater porosities, the non-linear inertial effects must be included. Predictions from this model, however, will only be accurate if the local Reynolds number is sufficiently small $Re_L < 10$, thus materials with large open pores may still not be suitably described.

We repeat the results for a NACA 4-digit aerofoil with 6% thickness in Figure 3 (right), and, as expected, observe similar trends to the constant thickness plate case. To investigate further the agreement with experimental results and the impact of plate thickness on trailing-edge noise, we plot the noise reduction in Figure 4 for Case 2 and Case 3. Here,

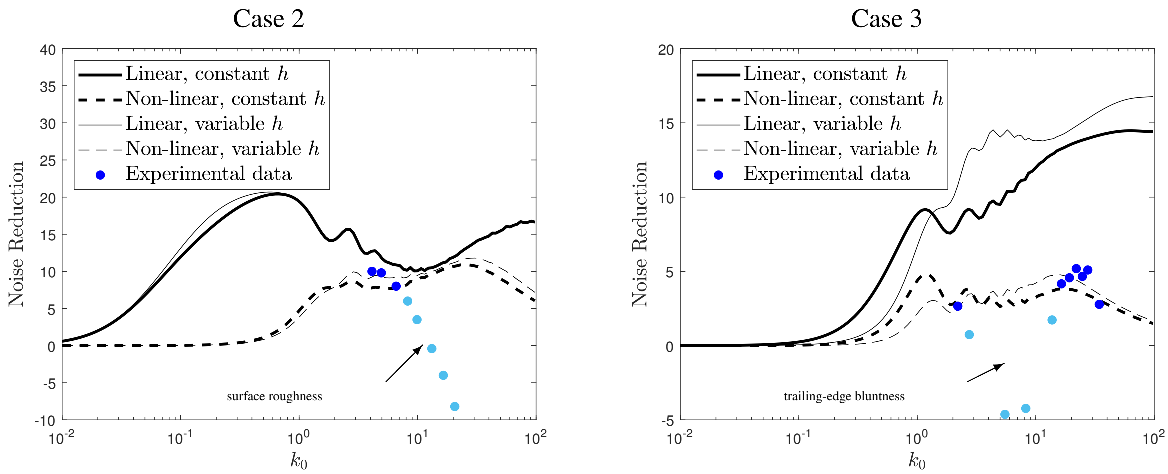

Fig. 4 Comparisons of noise reduction with experimental data from [1, 9].

a positive value indicates that the corresponding case is quieter than a fully impermeable plate of the same geometry by that many dB. The experimental data from [3, 9] are also plotted for the respective cases. The results of [9] provide only high-frequency data and therefore, are impacted by roughness noise. Data from [3] in Figure 4 (right) for Case 3 covers a wider range of comparable frequencies and, discounting the trailing-edge bluntness noise increase, we see very good agreement between the non-linear model and the experimental results. The linear model in contrast greatly over predicts the noise reduction similar to the Case 2 situation. Both Case 2 and Case 3 illustrate that the plate geometry has a minor effect on noise reduction for the non-linear case, but a more significant effect in just the linear case.

Finally, we consider what effect the non-linear boundary condition has on the far-field directivity and surface pressure jump. We consider Case 3, for which we know the Forchheimer model is well-suited. Figure 5 illustrates the pressure jump across $y = 0$ for a plate of constant thickness, alongside the far-field directivity (plotted on a log scale) for both linear and non-linear boundary conditions. For low frequencies ($k_0 = 0.1$), there is little difference between the linear and non-linear cases, and thus minimal impact of inertia. This is expected due to relatively low velocities. For higher frequencies and thus higher velocities, we see a higher trailing-edge peak surface pressure for the non-linear case, indicating that whilst viscosity dissipates pressure at the surface, inertial effects either hinder this viscous mechanism or independently amplify pressure. This has two effects on the far-field directivity. First, a higher overall surface pressure for the non-linear case results in a greater overall magnitude of far-field noise. Second, a higher peak trailing-edge pressure for the non-linear case results in a scattered field dominated by just the scattering at the trailing edge, and thus a reduced interference pattern in the far-field directivity when compared to the linear case. Similar effects are observed for the NACA 0006 profile in Figure 6, where the variable thickness plate also results in a more oscillatory surface pressure at high frequencies. This causes an increased interference-type pattern in far-field directivities, with the linear case being most impacted upon comparison to Figure 5.

V. Conclusion

We presented a low-fidelity numerical solution to rapidly predict aerofoil trailing-edge noise accounting for both linear viscous effects and non-linear inertial effects within metal foam-like porous materials. The linear model at high frequencies can hugely over-predict the noise reduction upon comparison with experimental data. However, when supplemented with a non-linear Forchheimer correction, we see good agreement in noise reduction predictions versus experimental data. Further comparisons with Large Eddy Simulations and experimental results corroborating this conclusion can be found in [19] (which also discusses extensions to multiple plates). The model allows constant or non-constant plate thickness. However, it requires the total thickness to be sufficiently small so that we may linearise the appropriate pressure jump condition to the chord line $y = 0$. We note that for quadrupole-type noise sources, the peak scattered pressure on the surface at the trailing edge is sufficiently dominant that the effects of altering the frontal section of the plate are minimal. Conversely, if only viscous (linear) effects are accounted for, significant attenuation of the source occurs at the trailing edge, and therefore the response along the full plate contributes to the far-field scattered noise. Variations in the boundary conditions along the plate, therefore, have a greater impact on the scattered noise.

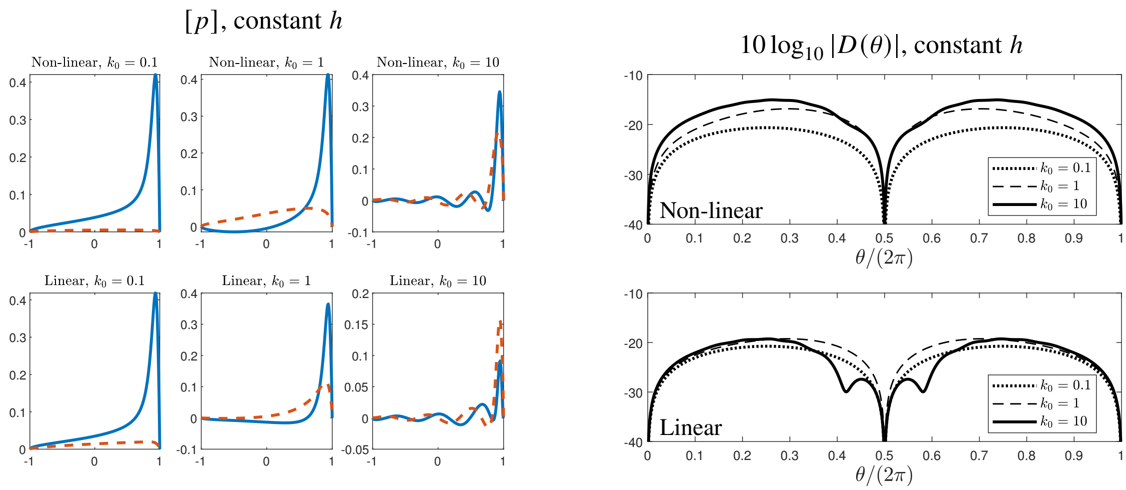

Fig. 5 Left: Surface pressure jump for different values of k_0. The real parts are shown as solid lines, whereas the imaginary parts are shown as dashed lines. Right: Far-field (log) directivity. In all cases, the plate thickness is constant, $h = 0.012$.

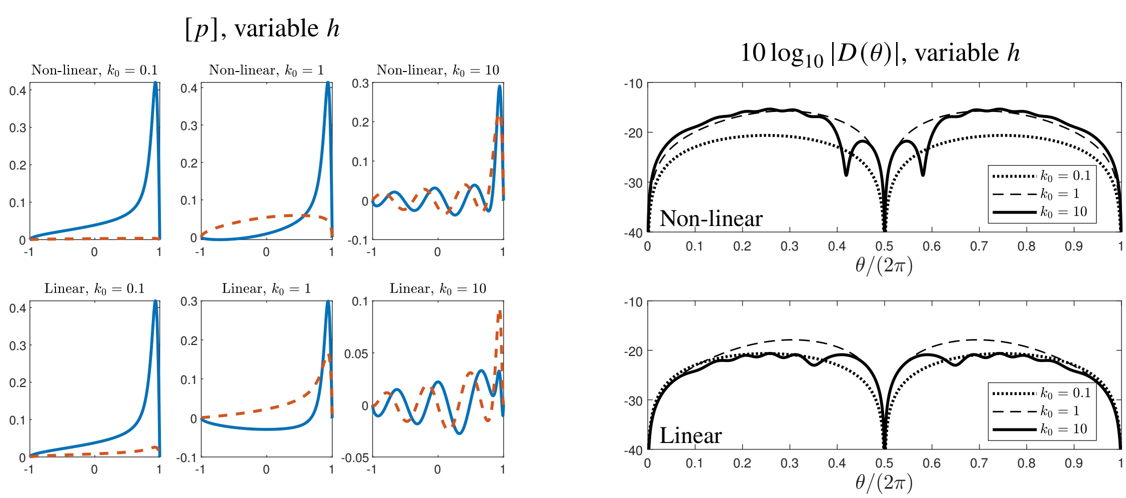

Fig. 6 Left: Surface pressure jump for different values of k_0. The real parts are shown as solid lines, whereas the imaginary parts are shown as dashed lines. Right: Far-field (log) directivity. In all cases the plate thickness takes a NACA 0006 profile.

We conclude that for mid and high frequencies and typical high permeability materials, the local inertial effects at the trailing edge can dominate the overall acoustic scattering behaviour. Thus accurate modelling of the realistic shape of the aerofoil is unnecessary in comparison to the importance of including the inertial effects of the material local to the source, in this case, the boundary layer.

Finally, we remark that it is not solely the permeability which determines the inertial effects, since an independent inertial coefficient in the Forchheimer model must also be provided to characterise the porous material. It may also be the case that this inertial coefficient is non-constant; many empirical formulae exist for permeable rocks [20]. However, the literature is less complete for the application considered here of metal foams in air. Since the model presented here can deal with non-constant coefficients, a variable Forchheimer coefficient could certainly be used should one be determined for a material of interest. This model further does not account for the impact of the rough porous surface on the generation of turbulence, and cannot capture any roughness noise measured experimentally. However, it may be possible to supplement this model with a prediction of surface roughness noise [21]. Another possible extension is to model non-linear inertial effects for elastic materials [22, 23].

References

[1] Geyer, T., Sarradj, E., and Fritzsche, C., "Measurement of the noise generation at the trailing edge of porous airfoils," *Exp Fluids*, Vol. 48, 2010, p. 291–308. https://doi.org/https://doi.org/10.1007/s00348-009-0739-x.

[2] Sarradj, E., and Geyer, T., "Symbolic regression modeling of noise generation at porous airfoils," *Journal of Sound and Vibration*, Vol. 333, No. 14, 2014, pp. 3189 – 3202. https://doi.org/https://doi.org/10.1016/j.jsv.2014.02.037, URL http://www.sciencedirect.com/science/article/pii/S0022460X14001783.

[3] Geyer, T., Sarradj, E., and Fritzsche, C., "Porous Airfoils: Noise Reduction and Boundary Layer Effects," *International Journal of Aeroacoustics*, Vol. 9, No. 6, 2010, pp. 787–820. https://doi.org/10.1260/1475-472X.9.6.787, URL https://doi.org/10.1260/1475-472X.9.6.787.

[4] Chaitanya, P., Joseph, P., Chong, T. P., Priddin, M. J., and Ayton, L. J., "On the noise reduction mechanisms of porous aerofoil leading edges," *Journal of Sound and Vibration*, Vol. 485, 2020, p. 115574. https://doi.org/https://doi.org/10.1016/j.jsv.2020.115574, URL http://www.sciencedirect.com/science/article/pii/S0022460X20304065.

[5] Jaworski, J. W., and Peake, N., "Aerodynamic noise from a poroelastic edge with implications for the silent flight of owls," *Journal of Fluid Mechanics*, Vol. 723, 2013, p. 456–479. https://doi.org/10.1017/jfm.2013.139.

[6] Rayleigh, L., *The Theory of Sound*, vol. 2. Dover, 1945.

[7] Howe, M. S., Scott, M. I., and Sipcic, S. R., "The influence of tangential mean flow on the Rayleigh conductivity of an aperture," *Proc. Roy. Soc. A*, Vol. 452, No. 1953, 1996, pp. 2303–2317. https://doi.org/10.1098/rspa.1996.0123.

[8] Howe, M. S., and Lighthill, M. J., "On the theory of unsteady high Reynolds number flow through a circular aperture," *Proceedings of the Royal Society of London. A. Mathematical and Physical Sciences*, Vol. 366, No. 1725, 1979, pp. 205–223. https://doi.org/10.1098/rspa.1979.0048, URL https://royalsocietypublishing.org/doi/abs/10.1098/rspa.1979.0048.

[9] Rubio Carpio, A., Avallone, F., Ragni, D., Snellen, M., and van der Zwaag, S., "Mechanisms of broadband noise generation on metal foam edges," *Physics of Fluids*, Vol. 31, No. 10, 2019, p. 105110. https://doi.org/10.1063/1.5121248, URL https://doi.org/10.1063/1.5121248.

[10] Cimolin, F., and Discacciati, M., "Navier–Stokes/Forchheimer models for filtration through porous media," *Applied Numerical Mathematics*, Vol. 72, 2013, pp. 205 – 224. https://doi.org/https://doi.org/10.1016/j.apnum.2013.07.001, URL http://www.sciencedirect.com/science/article/pii/S0168927413000913.

[11] Ayton, L. J., Colbrook, M. J., Geyer, T. F., Chaitanya, P., and Sarradj, E., "Reducing aerofoil–turbulence interaction noise through chordwise-varying porosity," *Journal of Fluid Mechanics*, Vol. 906, 2021.

[12] Colbrook, M. J., and Priddin, M. J., "Fast and spectrally accurate numerical methods for perforated screens (with applications to Robin boundary conditions)," *IMA Journal of Applied Mathematics*, Vol. 85, No. 5, 2020, pp. 790–821.

[13] Colbrook, M. J., and Kisil, A. V., "A Mathieu function boundary spectral method for scattering by multiple variable poro-elastic plates, with applications to metamaterials and acoustics," *Proceedings of the Royal Society A*, Vol. 476, No. 2241, 2020, p. 20200184.

[14] Ayton, L. J., Colbrook, M. J., and Fokas, A. S., "The Unified Transform: A Spectral Collocation Method for Acoustic Scattering," *25th AIAA/CEAS Aeroacoustics Conference*, 2019, p. 2528.

[15] Colbrook, M. J., "Mathieu Function Collocation," *github (online) https://github.com/MColbrook/MathieuFunctionCollocation*, 2020.

[16] Lighthill, M. J., "On sound generated aerodynamically I. General theory," *Proc. R. Soc. Lond. A*, Vol. 211, No. 1107, 1952, pp. 564–587. https://doi.org/10.1098/rspa.1952.0060.

[17] Colbrook, M. J., Ayton, L. J., and Fokas, A. S., "The unified transform for mixed boundary condition problems in unbounded domains," *Proceedings of the Royal Society A*, Vol. 475, No. 2222, 2019, p. 20180605.

[18] Zhong, W., Ji, X., Li, C., Fang, J., and Liu, F., "Determination of Permeability and Inertial Coefficients of Sintered Metal Porous Media Using an Isothermal Chamber," *Applied Sciences*, Vol. 8, No. 9, 2018. https://doi.org/10.3390/app8091670, URL https://www.mdpi.com/2076-3417/8/9/1670.

[19] Colbrook, M. J., and Ayton, L. J., "Do we need non-linear corrections? On the boundary Forchheimer equation in acoustic scattering," *Journal of Sound and Vibration*, Vol. 495, 2021, p. 115905.

[20] Takhanov, D., "Forchheimer model for non-Darcy flow in porous media and fractures," *MSc Thesis, Imperial College London*, 2011. URL https://spiral.imperial.ac.uk/bitstream/10044/1/24389/2/Takhanov-D-2011-Pet-Eng-MSc-thesis.pdf.

[21] Ayton, L. J., "Bioinspired aerofoil adaptations: The next steps for theoretical models," *Philosophical Transactions of the Royal Society A: Mathematical, Physical and Engineering Sciences*, Vol. 377, No. 2159, 2019, p. 20190070. https://doi.org/10.1098/rsta.2019.0070, URL https://royalsocietypublishing.org/doi/abs/10.1098/rsta.2019.0070.

[22] Cavalieri, A. V., Wolf, W. R., and Jaworski, J., "Acoustic scattering by finite poroelastic plates," *20th AIAA/CEAS Aeroacoustics Conference*, 2014, p. 2459. 00005.

[23] Colbrook, M. J., and Ayton, L. J., "A spectral collocation method for acoustic scattering by multiple elastic plates," *Journal of Sound and Vibration*, Vol. 461, 2019, p. 114904.

Acknowledgments

This work was supported by a Research Fellowship at Trinity College, Cambridge (M.J.C.) and an EPSRC Early-Career Fellowship EP/P015980/1 (L.J.A.).